Science Bulletin 70 (2025) 148–152

Contents lists available at ScienceDirect

Science Bulletin

journal homepage: www.elsevier.com/locate/scib

Short Communication

Over 200 times current enhancement via buckling triboelectric nanogenerator at ultra-low speed for monitoring the swelling of lithium ion batteries

Maoyi Zhang [a,b,c], Chaosheng Hu [a,d], Tongtong Zhang [a,d], Chris R. Bowen [e], Rui Li [f], YongAn Huang [g], Yewang Su [b,c,*], Zhong Lin Wang [a,d,h,*], Ya Yang [a,d,*]

[a] Beijing Key Laboratory of Micro-Nano Energy and Sensor, Center for High-Entropy Energy and Systems, Beijing Institute of Nanoenergy and Nanosystems, Chinese Academy of Sciences, Beijing 101400, China
[b] State Key Laboratory of Nonlinear Mechanics, Institute of Mechanics, Chinese Academy of Sciences, Beijing 100190, China
[c] School of Engineering Science, University of Chinese Academy of Sciences, Beijing 100049, China
[d] School of Nanoscience and Technology, University of Chinese Academy of Sciences, Beijing 100049, China
[e] Department of Mechanical Engineering, University of Bath, Bath BA27AK, UK
[f] State Key Laboratory of Structural Analysis for Industrial Equipment, Dalian University of Technology, Dalian 116024, China
[g] State Key Laboratory of Intelligent Manufacturing Equipment and Technology, Huazhong University of Science and Technology, Wuhan 430074, China
[h] School of Material Science and Engineering, Georgia Institute of Technology, Atlanta, GA 30332-0245, USA

ARTICLE INFO

Article history:
Received 25 June 2024
Received in revised form 16 September 2024
Accepted 10 October 2024
Available online 17 October 2024

Sensors deployed within the Internet of Things (IoT) require a stable and continuous electrical energy supply [1]. The traditional approach to provide an energy supply relies primarily on battery power, which has specific shortcomings; these include integration difficulties, the need for frequent charging or replacement, and environmental pollution associated with battery production and disposal. To solve the challenge of delivering an energy supply to sensors, researchers have designed self-powered sensors or have produced power for sensors by scavenging mechanical energy from the surrounding environment. Electromagnetic generators [2], piezoelectric generators [3] and triboelectric nanogenerators (TENGs) [4,5] are common approaches to scavenge mechanical energy. TENGs have been widely used in the development of self-powered sensors and the supply of electrical energy to sensors due to their high performance, low cost, and wide range of potential materials [6].

The current output of a TENG is related to the speed of motion [7,8], where the slower the speed, the smaller the current generated. As a result, during operation in ultra-low speed environments (<10 mm s^{-1}), the current output of a TENG will be small, which greatly limits the applications of TENGs. Previous researchers have designed TENGs with an instantaneous release of elastic energy using elastomers [9,10], which can convert ultra-low motion into high speed motion. The lowest speed they tested was approximately 30 mm s^{-1}. In this work, we develop a structure that not only exhibits a high current density at lower speeds (0.05 mm s^{-1}) but is also simple, greatly enhancing the application potential of TENG in ultra-low speed environments.

We propose here a novel strategy based on a buckling effect that is able to convert an ultra-low speed motion into a high-speed motion to enhance the current output by development of a buckling TENG (B-TENG) with a simple structure. The B-TENG achieves a current enhancement of over 200 times compared to a conventional TENG (C-TENG) when operating at an ultra-low speed of 0.2 mm s^{-1}. The B-TENG achieves a current density of 14.3 mA mm^{-2} at an ultra-low speed of 0.05 mm s^{-1}. The mechanism of the current enhancement of the B-TENG is explored in detail.

High operating temperatures and improper cyclic charging and discharging can lead to lithium ion battery (LIB) swelling (Fig. S1 online). LIB swelling is an inherently ultra-low speed process, and the B-TENGs are employed as self-powered sensors to monitor LIB swelling. This work therefore breaks a new path for the design of ultra-low speed TENGs.

Fig. 1a compares the device architecture of a C-TENG and B-TENG. While both friction layers of a C-TENG have a planar structure, the B-TENG replaces one of the friction layers with a curved

* Corresponding authors.
E-mail addresses: yewangsu@imech.ac.cn (Y. Su), zhong.wang@mse.gatech.edu (Z.L. Wang), yayang@binn.cas.cn (Y. Yang).

https://doi.org/10.1016/j.scib.2024.10.014

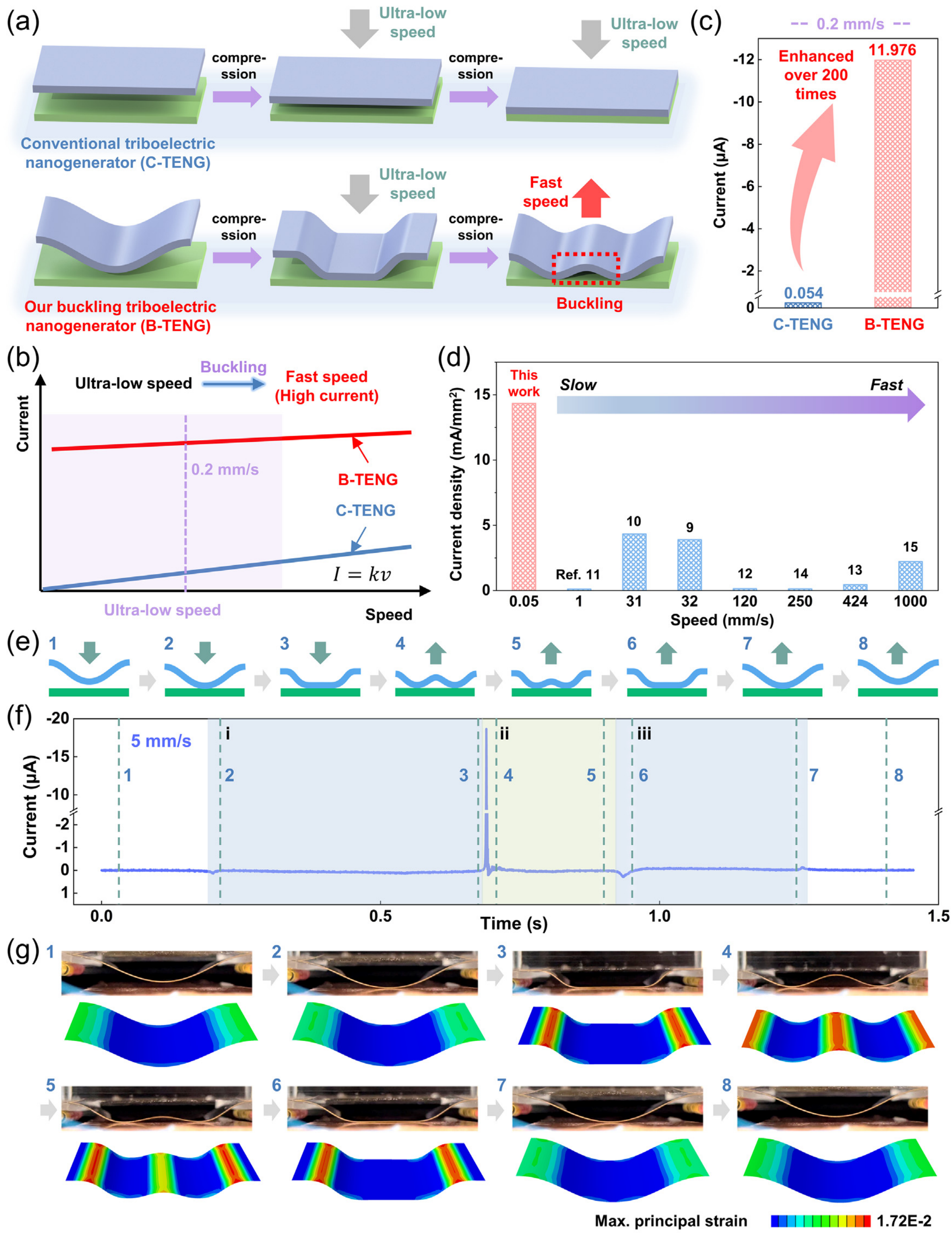

Fig. 1. Working mechanism and superiority of B-TENG. (a) Contact behavior of C-TENG and B-TENG at ultra-low speed. (b) Schematic of current output with respect to speed for C-TENG and B-TENG. (c) Comparison of current output of B-TENG and C-TENG at ultra-low speed of 0.2 mm s^{-1}. (d) Comparison of current density at minimum speed of B-TENG with different TENGs. (e) Deformation states of B-TENG under a complete motion period. (f) Current waveform of B-TENG and (g) physical diagram of the curved structure and the corresponding strain distribution of polyimide under a complete motion period at 5 mm s^{-1}.

structure. When the planar C-TENG layers make contact at an ultra-low speed, the current of C-TENGs will also be small. However, when the B-TENG layers make contact at an ultra-low speed, the two layers are in face-to-face contact at the beginning of a cycle. As the two layers of the B-TENG approach each other further, the region of the curved structure that is in contact with the flat structure will suddenly buckle and bulge in the opposite direction at a high speed. The rapid rate of deformation as a result of the buckling event results in an enhancement of the current output. The understanding of buckling behavior is described in detail in the Supplementary materials Note S1. Fig. 1b is a schematic diagram of current output with respect to speed for C-TENG and B-TENG. The current of C-TENG is proportional to the speed, so that the current of the C-TENG will also be small in an ultra-low speed environment. In contrast, the B-TENG converts ultra-low speed motion to fast motion through buckling, so that the B-TENG produces a high current in an ultra-low speed environment. The B-TENG achieves a current enhancement of over 200 times compared to the C-TENG when operating at an ultra-low speed of 0.2 mm s^{-1} (Fig. 1c).

Fig. 1d demonstrates a comparison of the measured current densities of the B-TENG and different TENGs at the minimum speed [9–15]. At speeds of 32 and 31 mm s^{-1} [9,10], there is a large increase in current density compared to the reported literature at greater speeds. This is because the TENGs were designed with an instantaneous release of elastic energy using elastomers, which can convert ultra-low speed motion into high speed motion. In the reported work at a lower speed of 1 mm s^{-1} with a current density of 0.11 mA mm^{-2}, a direct-current TENG was designed to exhibit a measurable current density due to breaking of the surface charge density limit of air breakdown [11]. In this work, 0.05 mm s^{-1} is the minimum speed of the B-TENG with a steady and high current signal (Fig. S7 online). The current is 11.47 μA and the current density is 14.3 mA mm^{-2}. The minimum speed of the B-TENG is not only much smaller than that reported in other works shown in Fig. 1d, but also its current density is much larger. This proves that B-TENG exhibits much improved performance compared to other TENGs in an ultra-low speed environment. The structure of B-TENG is described in detail in the Supplementary materials Note S2.

The current output and the deformation state of the B-TENG are closely related. Fig. 1e and f demonstrate the deformation and the corresponding current waveform of the B-TENG for a complete motion period at 5 mm s^{-1}, respectively. The time period from the initial contact between the curved structure and the planar structure until the onset of buckling is termed *stage i*. The time when buckling occurs until the buckled region disappears is termed *stage ii*. It can be seen that the high speed of the buckling event results in a large current peak. The time from the disappearance of the bulge to the complete separation of the two is termed *stage iii*. A detailed description of the three stages is provided in the Supplementary materials Note S3. Fig. 1g shows the physical diagram of the curved structure and the strain distribution of the polyimide throughout the period, where the deformation contours of the finite element analysis are in excellent agreement with the physical observations. The strain induced by the reverse bulge is large where the larger the reverse bulge, the greater the level of strain. The effect of different speeds on the waveform produced is described in the Supplementary materials Note S4.

The interval time has an effect on the electrical output of the B-TENG, where the interval time represents the time between two occurrences of buckling by the B-TENG. In the case of a short interval time, the current of the B-TENG is attenuated, as seen in Fig. 2a and b. Whereas, in the case of a long interval time between individual buckling events, there is no attenuation of the current produced by the B-TENG. The speed of motion was maintained at 5 mm s^{-1}, and the interval time was varied by increasing the pause time between each separation event. With an interval time ranging from 2 to 30 s, an attenuation of the current can be observed and the longer the interval time, the lower the attenuation of the current. At an interval time of 30 s, the current decreases to a certain extent and then enters a platform period without a further decrease. At the longer interval times of 60 and 120 s, there is no current attenuation.

The effect of different interval times on the B-TENG is a consequence of the viscoelastic nature of polyimide, a widely used polymer material. All polymer materials exhibit a degree of viscoelasticity, which results in the time required to recover to the initial state after unloading. The mechanism by which viscoelasticity affects current in the time interval is described in the Supplementary materials Note S5.

The viscoelasticity of a material is also affected by the speed of deformation of the material, where the lower the deformation rate, the longer it takes to recover to the initial state. The speed of deformation in this regard corresponds to the speed of the B-TENG surfaces, and the effect of different speeds on the electrical response of the B-TENG was investigated. The current is observed to increase with an increase in speed (Fig. 2c), which indicates that the approach speed affects the buckling speed. An attenuation of the current can be observed when the speed is 0.1 (Video S1 online), 0.2, and 0.5 mm s^{-1}. The smaller the approach speed, the more severe the attenuation of the current, which is consistent with the predicted trend that viscoelasticity is affected by the rate of deformation and is further evidence that the current attenuation is the result of a viscoelastic response. At low speeds of 0.2 and 0.5 mm s^{-1}, a platform period of current attenuation is observed. When the speed is greater than or equal to 1 mm/s, no current attenuation is observed. On increasing the interval time from 80 to 500 s, the currents were investigated at speeds of 0.1, 0.05, and 0.02 mm s^{-1} (Fig. S7 online). As the speed decreases, the current attenuation becomes more severe due to the significant increase in the interval time. A platform period of current attenuation can be observed at a speed of 0.1 mm s^{-1}.

The C-TENG was measured at different speeds under the same conditions as the B-TENG. The currents of the B-TENG and the C-TENG are compared at different speeds, see the inset in Fig. 2d. The current produced by the C-TENG increases linearly as the speed increases, which is consistent with theory [7,8]. Since the current of the C-TENG is too small to be measured at lower speeds, the lowest speed at which the current of the C-TENG was measured was 0.2 mm s^{-1}. The degree of current enhancement of B-TENG, relative to C-TENG, at different speeds is shown in Fig. 2d. At a speed of 0.2 mm s^{-1}, the current produced by the B-TENG is over 200 times greater that of the C-TENG.

The effect of different heights of the curved structure on the current was investigated. As shown in Fig. 2e, the current increases as the height of the curved structure increases. The results of finite element simulation show that the strain increases with increasing height, see Fig. S8a (online). The larger the strain, the larger the force required to trigger buckling, which results in a faster speed of buckling and therefore a higher current. Different thicknesses of the curved structure were also investigated to study its effect on the current output. As the thickness increases, the current increases (Fig. 2f) and the finite element simulations show the thicker the thickness, the larger the strain (Fig. S8b online).

We now simulate the phenomenon of LIBs swelling by heating. Fig. 2g shows a physical diagram of the monitoring of swelling of LIBs using a C-TENG. The monitoring results are shown in Fig. 2h, and the C-TENG is unable to monitor the signal of LIB swelling since the speed of LIB swelling is too slow for this device configuration. However, the B-TENG was able to successfully monitor LIB swelling, as seen in Fig. 2h. A physical diagram after swelling showed that the B-TENG buckled (Fig. 2g), and the process of LIB monitoring swelling by both a C-TENG and B-TENG is shown in Video S2 (online). The B-TENG can also be applied to monitor the swelling of LIB arrays. Details of the experiment are in the Supplementary materials Note S6.

This work has developed a new strategy to convert an ultra-low-speed motion into a high-speed motion via a buckling to create a B-TENG which enhances the current output for sensing applications. The unique design of the B-TENG enables an enhancement of the current output by over 200 times compared to a C-TENG at a low displacement rate of 0.2 mm s^{-1}. The B-TENG achieves a current density of 14.3 mA mm^{-2} at an ultra-low speed of 0.05 mm s^{-1}. The mechanism of the B-TENG, which utilizes buckling to enhance the output current, is explored in detail by both experimental and numerical analysis, where the effects of interval time, approach speed and geometry on the B-TENG current are studied. To demonstrate the applicability of the novel design at low dis-

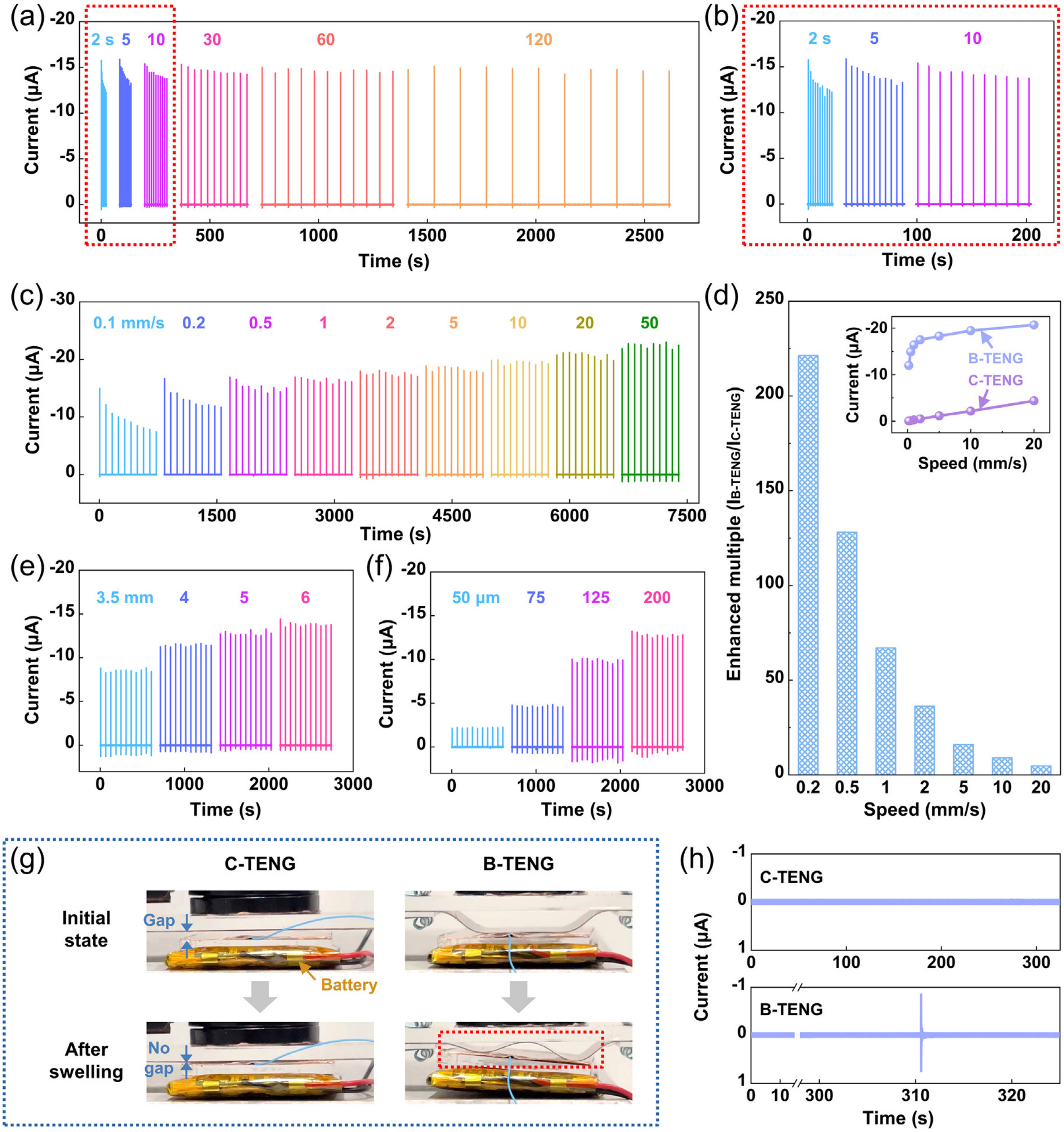

Fig. 2. Effect of different parameters on B-TENG current and monitoring of LIB swelling. (a, b) Current of B-TENG at different interval times. (c) B-TENG current at speeds from 0.1 to 50 mm s^{-1} when the time interval is 80 s. (d) Current enhancement of B-TENG relative to C-TENG at different speeds. The inset is comparison of current between B-TENG and C-TENG at different speeds. (e) Current of B-TENG at different heights. (f) Current of B-TENG at different thicknesses. (g) Physical diagrams and (h) currents of C-TENG and B-TENG monitoring of LIB swelling.

placement rates, the B-TENG is successfully utilized as a self-powered sensor to monitor the swelling of LIBs. This work therefore breaks a new path for the design of ultra-low speed TENGs.

Conflict of interest

The authors declare that they have no conflict of interest.

Acknowledgments

This work was supported by the National Key R&D Project from the Minister of Science and Technology in China (2021YFA1201604), the National Natural Science Foundation of China (52072041), the Beijing Natural Science Foundation (JQ21007), the University of Chinese Academy of Sciences (Y8540XX2D2), Opening fund of State Key Laboratory of Nonlinear Mechanics (LNM202207), State Key Laboratory of Intelligent Manufacturing Equipment and Technology, Huazhong University of Science and Technology (DMETKF2022014), State Key Laboratory of Structural Analysis for Industrial Equipment, Dalian University of Technology (GZ22102), the National Natural Science Foundation of China (12172359), Key Research Program of Frontier Sciences of the Chinese Academy of Sciences (ZDBS-LY-JSC014), and CAS Interdisciplinary Innovation Team (JCTD-2020-03).

Author contributions

Yewang Su, Zhong Lin Wang, and Ya Yang conceived the idea and supervised the research. Maoyi Zhang, Chaosheng Hu, and Tongtong Zhang carried out the device fabrication and the performance measurements of the devices. Maoyi Zhang, Chris R. Bowen, Rui Li, YongAn Huang, Yewang Su, Zhong Lin Wang, and Ya Yang analyzed the data. Maoyi Zhang, Chris R. Bowen, Yewang Su, Zhong Lin Wang and Ya Yang co-wrote the manuscript.

Appendix A. Supplementary material

Supplementary data to this article can be found online at https://doi.org/10.1016/j.scib.2024.10.014.

References

[1] Wang ZL. Entropy theory of distributed energy for internet of things. Nano Energy 2019;58:669–72.
[2] Zhang T, Kong L, Zhu Z, et al. An electromagnetic vibration energy harvesting system based on series coupling input mechanism for freight railroads. Appl Energy 2024;353:122047.
[3] Su C, Huang X, Zhang L, et al. Robust superhydrophobic wearable piezoelectric nanogenerators for self-powered body motion sensors. Nano Energy 2023;107:108095.
[4] Li X, Luo J, Han K, et al. Stimulation of ambient energy generated electric field on crop plant growth. Nat Food 2022;3:133–42.
[5] Fan FR, Tian ZQ, Wang ZL. Flexible triboelectric generator. Nano Energy 2012;1:328–34.
[6] Cao X, Xiong Y, Sun J, et al. Multidiscipline applications of triboelectric nanogenerators for the intelligent era of internet of things. Nano-Micro Lett 2023;15:14.
[7] Niu S, Wang ZL. Theoretical systems of triboelectric nanogenerators. Nano Energy 2015;14:161–92.
[8] Niu S, Wang S, Lin L, et al. Theoretical study of contact-mode triboelectric nanogenerators as an effective power source. Energy Environ Sci 2013;6:3576–83.
[9] Xu Z, Li D, Wang K, et al. Stomatopod-inspired integrate-and-fire triboelectric nanogenerator for harvesting mechanical energy with ultralow vibration speed. Appl Energy 2022;312:118739.
[10] Liu G, Leng Q, Lian J, et al. Notepad-like triboelectric generator for efficiently harvesting low-velocity motion energy by interconversion between kinetic energy and elastic potential energy. ACS Appl Mater Interfaces 2015;7:1275–83.
[11] Zhang J, Gao Y, Liu D, et al. Discharge domains regulation and dynamic processes of direct-current triboelectric nanogenerator. Nat Commun 2023;14:3218.
[12] Li G, Wu H, Guo R, et al. A triboelectric piston–cylinder assembly with condition-monitoring and self-powering capabilities. Energy Tech 2022;10:2200014.
[13] Long L, Liu W, Wang Z, et al. High performance floating self-excited sliding triboelectric nanogenerator for micro mechanical energy harvesting. Nat Commun 2021;12:4689.
[14] Wang K, Zhou J, Ouyang H, et al. A dual quasi-zero-stiffness sliding-mode triboelectric nanogenerator for harvesting ultralow-low frequency vibration energy. Mech Syst Signal Process 2021;151:107368.
[15] Li XH, Han CB, Zhang LM, et al. Cylindrical spiral triboelectric nanogenerator. Nano Res 2015;8:3197–204.